Journal of Asian Earth Sciences 172 (2019) 443–457

Contents lists available at ScienceDirect

Journal of Asian Earth Sciences

journal homepage: www.elsevier.com/locate/jseaes

Full length article

A statistical space-time-magnitude analysis on the aftershocks occurrence of the July 21th, 2017 $M_W = 6.5$ Bodrum-Kos, Turkey, earthquake

Serkan Öztürk[a,*], Şakir Şahin[b]

[a] Gümüşhane University, Department of Geophysics, 29100 Gümüşhane, Turkey
[b] Süleyman Demirel University, Department of Geophysics, 32260 Isparta, Turkey

ARTICLE INFO

Keywords:
Aftershock hazard
Bodrum-Kos earthquake
Fractal dimension
Gutenberg-Richter relation
The modified Omori law

ABSTRACT

In this study, a detailed space-time-magnitude assessment on the aftershock sequence of July 21th, 2017, M_W 6.5, Bodrum-Kos earthquake (Turkey) is carried out by focusing on the analyses of aftershock parameters: *b*-value, *p*-value, *Dc*-value and Mamax. *b*-value is estimated as 0.90 ± 0.05 with a completeness magnitude $Mc = 1.6$ and this relatively small *b*-value may be resulted from the abundance of aftershocks with magnitude $M_L \geq 4.0$. However, it is well represented by the Gutenberg-Richter law with a typically $b \approx 1.0$. *p*-value is estimated as 1.04 ± 0.02 with a *c*-value = 0.224 ± 0.039 and is well characterized nearly close to the global $p \approx 1.0$. This relatively high *p*-value may be a result of the relative fast decay rate of the aftershock activity. *Dc*-value is calculated as 1.74 ± 0.09 and it means that aftershocks are homogeneously distributed. Temporal distribution of *b*-value shows that small *b*-values may be due to a stepwise increase in effective stress before the occurrence of larger aftershocks. Regional changes range from 0.5 to 1.2 in *b*-value, from 0.4 to 1.3 in *p*-value and from 3.0 to 5.2 in Mamax. The smallest *b*-values are found in and around mainshock, including Karaada, Bodrum, Akyarlar and Turgutreis, and these regions have high stress as well as coseismic deformation. The largest *p*-values are found in and around the mainshock epicenter including Karaada, and it is interpreted that this situation may be caused by coseismic deformation. Mamax values larger than 4.4 are observed in and around mainshock epicenter, including Bodrum and Akyarlar, and there is a clear correlation between spatial variations of *b*-values and Mamax. These results show that stress changes and coseismic deformation seem highly effective on *b* and *p*-value variations. Therefore, a special interest needs to be given to these anomaly regions since aftershock hazard is highly associated with these parameters and may be developed considering their space-time-magnitude distribution.

1. Introduction

Aftershock sequences are generally considered as a significant part of the earthquake occurrences, because a strong mainshock can produce a large number of aftershocks in a short time and in a small region. Many aftershocks are located in and around fault rupture region after a mainshock. The largest aftershocks can be dangerous since they are not generally forecastable and thus, they have a potential for structural damage (Zhang et al., 2013). Space-time-magnitude distributions of aftershocks can provide a detailed knowledge on the Earth's crust, geometry of the fault, stress distribution associated with the earthquake occurrence, physical properties of the materials in the fault zone and source properties of large earthquakes (Polat et al., 2002; Bayrak and Öztürk, 2004; Ansari, 2017). In addition to these scientific acquisition from aftershock behaviors, practical applications for the analyzing of aftershock sequences can be preferred since large aftershock occurrence may supply several important further seismic hazard assessments on the minimization of the human victims, property damage, and social and economic disruption. The tectonic structure and the faulting mode are factors other than the fault surface properties that might control the aftershock behavior (Kisslinger and Jones, 1991). Therefore, a detailed evaluation of aftershock occurrences can give significant and interesting results for protecting against and mitigating earthquake disasters (Hu et al., 2013). If an earthquake with magnitude $M \geq 8.0$ occurs, an aftershock sequence following this large earthquake can produce one or a few aftershocks with $M \geq 7.0$, and this occurrence implies an additional significant earthquake hazard (Nuannin et al., 2012). For these reasons, many researchers have drawn attention to the importance of statistical and physical assessments of the mainshock-aftershock pattern to seismic hazard evaluations. These types of studies have been gained

* Corresponding author at: Gümüşhane University, Department of Geophysics, TR-29100 Gümüşhane, Turkey.
E-mail address: serkanozturk@gumushane.edu.tr (S. Öztürk).

https://doi.org/10.1016/j.jseaes.2018.10.008
Received 14 May 2018; Received in revised form 26 September 2018; Accepted 16 October 2018
Available online 17 October 2018

more attention in recent years and a number of detailed papers on this subject by different authors for different aftershock sequences appeared for different parts of the word (e.g., works by Ranalli, 1969; Wiemer, and Katsumata, 1999; Ogata, 2001; Enescu and Ito, 2002; Polat et al., 2002; Bayrak and Öztürk, 2004; Daniel et al., 2006; Öztürk et al., 2008; Enescu et al., 2011; Nuannin et al., 2012; Zhang et al., 2013; Nemati, 2014; Ávila-Barrientos et al., 2015; Hainzl et al., 2016; Wei-Jin and Jian, 2017; Ansari, 2017). These analyses have revealed that activity, energy release and decay rate of aftershock sequences show significant changes in space-time domain in each aftershock sequence following the mainshock. According to these studies, all aftershock patterns can be considered as correlated with tectonic characteristics such as rheology, thickness, age, among others (Ávila-Barrientos et al., 2015). Thus, the aftershocks give an important seismic hazard, which sometimes can even improve the mainshock hazard.

The Aegean region and western part of Turkey show complex tectonic structures due to the strong heterogeneity in the crust. Main tectonics have been progressed as a result of the northward movements of the African and Arabian plates relative to the Eurasian plate, and following counter-clockwise rotation of the Anatolian Block since Miocene. Tectonic structures and related complex deformations due to the African-Eurasian convergence are also related to intense earthquake activity which includes many strong or destructive events in and around this region (Yolsal-Çevikbilen et al., 2014). A detailed study for Pliocene-Quaternary tectonic evolution of the Gökova Gulf was given by Tur et al. (2015). Geological formations in the surrounding area of Gökova Gulf are composed of metamorphic units in Neogene and middle-upper Miocene volcanics in Bodrum peninsula, located in the north of Gökova Gulf. However, in Datça peninsula in the southern part of Gökova Gulf, Ophiolitic units in Neogene and sedimentary units can be extensively seen. One can find many details in Tur et al. (2015) for the geological structure of Bodrum-Kos aftershock region.

A large earthquake with moment magnitude Mw = 6.5 (local magnitude M_L = 6.2) at a depth of 19.44 km which has a normal faulting mechanism striking about east-west occurred on July 21th, 2017 in Gökova Bay (Aegean Sea) at local time 01:31:09 (UTC) between Bodrum town, Turkey, and Kos island, Greece (AFAD, Disaster and Emergency Management Authority). According to the AFAD records, mainshock epicenter was given as 36.9198°N and 27.4435°E located 12 km to Kos in Greece and 8 km to Bodrum (Muğla) in Turkey. The earthquake was highly felt in the southwestern Aegean Region, especially in Muğla province. The earthquake caused a tsunami which affected the coast of Bodrum peninsula and the northeast coast of Kos island. The tsunami was recorded by a tide gauge, located in Bodrum, close to the earthquake epicenter (Yalçıner et al., 2017). In this study, we evaluated the statistical properties of aftershock sequence of Bodrum-Kos earthquake that occurred on July 21th, 2017 in the western part of Turkey. The objective of this study is to present a detailed region-time-magnitude analysis including several aftershock parameters such as the *b*-value of the frequency-magnitude distribution, the *p*-value of the modified Omori law and *Dc*-value of the fractal dimension for 10,600 aftershocks identified in six months after the mainshock. All calculations of aftershock parameters were made by applying the ZMAP software package (version 6, Wiemer, 2001). The results obtained in this study have a significance not only for the space-time-magnitude characteristics of the aftershock sequence but also help to understand the generation of aftershock occurrences. Statistical properties of aftershocks also make a contribution to attempts to forecast aftershock activities following large mainshocks and can be used to reveal the seismic hazard in this region.

2. Methods

Statistical characteristics of aftershock occurrences can give valuable and reliable information about the fault structure, cracks distribution, earthquake migration and the state of stress in the crust. Although there are numerous ways to describe the aftershock activity from a mainshock, aftershock characteristics can be described in space (fractal dimension, Grassberger and Procaccia, 1983), time (modified Omori law, Utsu et al., 1995) and magnitude (Gutenberg-Richter law, Gutenberg and Richter, 1944). These statistical models are the best known and the most common among different relationships defining the aftershock activity. One of the most effective tool to analyze the space-time-magnitude distribution of the aftershock sequence is to estimate the fractal dimension which may be used as a quantitative measure of the heterogeneity degree of earthquake activity in a region, and can be controlled by the heterogeneity of the stress field and the pre-existing geological structures (Öncel et al., 1996). Another way can be given as the Gutenberg-Richter (G-R) scaling law which describes the relationship between the frequency of occurrence and aftershock magnitudes. Thus, this power-law distribution can be applicable to aftershock magnitude-frequency analysis. The third basic model is the modified Omori law satisfying the temporal decay of aftershock sequence in many instances. The spatial distribution of the temporal decay of aftershocks may reflect either regional changes in the state of stress in the Earth or the material properties (e.g., Wiemer and Katsumata, 1999; Enescu and Ito, 2002; Polat et al., 2002; Bayrak and Öztürk, 2004; Öztürk et al., 2008; Nuannin et al., 2012; Arora et al., 2017).

2.1. Gutenberg-Richter relation (b-value)

Gutenberg and Richter (1944) relation describes the cumulative earthquake-size distribution in any region. The relationship between the frequency of occurrence and magnitude of aftershocks can be given with the following empirical equation:

$$\log_{10} N(M) = a - bM \tag{1}$$

where *N(M)* is the cumulative number of aftershocks with magnitudes equal to or greater than *M*, *a* and *b* values are positive constants. *a*-value describes the earthquake activity level and shows significant changes from region to region because it depends on observation period and investigation area. *b*-value describes the frequency-magnitude distribution of aftershocks, and tectonic structure of study region effects the spatial and temporal variations of *b*-value. The estimated *b*-value changes mostly between 0.6 and 1.4 (Wiemer and Katsumata, 1999). Utsu (1971) also stated that *b*-values vary roughly from 0.3 to 2.0, depending on the study region. Many factors can cause perturbations of the normal *b*-value. There a negative correlation between *b*-value and differential stress, and *b*-value defines the ratio between the relative proportion of small and great events in the region (Scholz, 2015; Ansari, 2016). The differential stress is a parameter strongly controlling faulting types, thus effecting the variations in *b*-value (Schorlemmer et al., 2005). In addition, *b*-value describes the magnitude distribution for a particular time interval, which can be used for estimation of seismic hazard. However, the physical implication of the *b*-value is not as obvious and is still under investigation.

2.2. Modified Omori law (p-value)

The occurrence rate of aftershock sequence as a function of time can be empirically defined by the modified Omori law (e.g., Utsu et al., 1995). The number of aftershocks increases suddenly after a mainshock and then decreases with time after the mainshock according to the modified Omori law which can be described by a following power law:

$$n(t) = \frac{K}{(t + c)^p} \tag{2}$$

where *n(t)* is the occurrence rate of aftershocks (number of aftershocks/day) per unit time, *t*-days after the mainshock. *K*, *p*, and *c* values are empirically derived positive constants which depend on the total number of events in the sequence and the activity rate in the earliest

part of the sequence, respectively. *K*-value is controlled by the total number of the aftershocks in the sequence. *K*-value, also called as aftershock productivity, is a normalizing parameter that is dependent on the total number of aftershocks and the threshold magnitude (Kisslinger and Jones, 1991; Ansari, 2017). *c*-value is generally considered as a delay between the mainshock rupture end and the start of the power law aftershock decay rate (Narteau et al., 2009). Therefore, *c*-value depends on the rate of activity in the earliest part of the sequences. *c*-value is a controversial quantity (Utsu et al., 1995) and strongly effected by incomplete detection of small aftershocks in the early stage of sequence (Kisslinger and Jones, 1991). *c*-value increases with the lower magnitude threshold of the considered aftershocks and has a non-zero value (Davidsen et al., 2015). Among these three parameters, *p*-value is the most important and defines the mode of aftershock decay as a function of time on frequency (Nanjo et al., 1998). Large *p*-value is expressed for fast decay whereas low *p*-value means slow decay of aftershock sequences. Many researchers have suggested that *p*-value usually changes between 0.5 and 1.8 for different aftershock sequences (e.g., Utsu et al., 1995; Olsson, 1999; Wiemer and Katsumata, 1999; Enescu and Ito, 2002; Polat et al., 2002; Bayrak and Öztürk, 2004). This variability may be associated with the tectonic conditions of the region such as fault heterogeneity, stress, and crustal heat flow. *p*-value can also provide quantitatively information about the fractal property of a pre-existing fault system in the crust but it is not clear which condition among them is more related to the *p*-value.

2.3. Fractal dimension (Dc-value)

Fractal concept has been used for a long time in order to describe the complexity of fault systems in which is observed the region and laboratory. The principal characteristics of a system of process which have fractal features are scale invariance or self-similarity. Fractal distribution of the earthquakes shows that the number of events greater than a specified magnitude has a power law dependence on the size. Fracture systems including fault systems have a statistical self-similar structure over a wide range of size scales through the fractal geometry concept introduced by Mandelbrot (1982) and extended by Turcotte (1992). Thus, fracture systems are characterized by a power law, with a characteristic exponent called a fractal dimension, *Dc*-value, and this parameter is widely used in seismology, especially to regional distribution of epicenters. One of the most commonly used methods for the calculation of fractal dimension is the correlation integral technique owing to its greater reliability and sensitivity to small variations in clustering features of points such as epicenters (Kagan and Knopoff, 1980; Öncel and Wilson, 2002). The correlation dimension method measures the spacing between two points. Fractal dimension of the spatial distribution of aftershocks occurrence can be defined by using two-point correlation dimension, *Dc*, and correlation sum *C*(*r*) given by (Grassberger and Procaccia, 1983):

$$Dc = \lim_{r \to 0} [\log C(r) / \log r] \tag{3}$$

$$C(r) = 2N_{R<r}/N(N-1) \tag{4}$$

where *C*(*r*) is the correlation function, *r* is the distance between two epicenters and *N* is the number of aftershocks pairs separated by a distance $R < r$. If the epicenter distribution has a fractal structure, following equation can be given:

$$C(r) \sim r^{Dc} \tag{5}$$

where *Dc* is a fractal dimension, more definitely, the correlation dimension. The distance *r* (in degrees) between two aftershocks is computed from:

$$r = \cos^{-1}(\cos\theta_i \cos\theta_j + \sin\theta_i \sin\theta_j \cos(\phi_i - \phi_j)) \tag{6}$$

where (θ_i, ϕ_i) and (θ_j, ϕ_j) are the latitudes and longitudes of the *i*th and *j*th aftershocks, respectively (Hirata, 1989). Fractal dimension is described by fitting a straight line by plotting *C*(*r*) against *r* on a double logarithmic coordinate, and is practically estimated from the slop of the straight line.

It has been accepted that earthquake distributions are fractal, and fractal dimension of earthquakes is a measure of the complexity in the earthquake occurrence and the clustering of earthquakes (Öncel et al., 1996). Hence, fractal analysis based on the correlation integral can be used to evaluate the regional features of the aftershock sequence. The fractal dimension varies from 0 to 2 related to the seismogenically active regions (Tosi, 1998). If *Dc*-value is close to zero, it may be interpreted as all aftershocks clustered into one point. If *Dc*-value is close to 1, it indicates the dominance of line sources. If *Dc*-value is close to 2, it indicates the planar fractured surface being filled-up. If *Dc*-value is close to 3 it indicates that earthquake fractures are filling up a crustal volume (Yadav et al., 2011, 2012). Also, if *Dc* value is close to 2, it is suggested that the earthquake epicenters are homogeneously distributed over a two-dimensional fault plane (Hirata, 1989; Yadav et al., 2011; Pailoplee and Choowong, 2014). Hence, fractal dimension may be estimated in order to avoid the possible unbroken fields, and these unbroken regions are suggested as potential seismic gaps to be broken in the future (Toksöz et al., 1979). Moreover, it has been observed in many studies that there is a negative correlation between *Dc*-value and *b*-value. Larger *Dc*-value associated with smaller *b*-value is the dominant structural feature in the regions of increased complexity in the active fault system. Also, it can be an indication of stress changes in the region (Öncel and Wilson, 2002; Polat et al., 2008).

3. Definition of aftershock sequence of July 21th, 2017 Bodrum-Kos earthquake

A detailed statistical analysis on space-time-magnitude distribution of aftershock sequence of the July 21th, 2017 Bodrum-Kos earthquake (Mo = 1.105×10^{19} Nm, from U.S. Geological Survey), Turkey was achieved in this study. The aftershock area is selected by considering the reports and studies from different researchers and institutions. It covers the region between the coordinates by longitudes 27.0°E–28.5°E, and latitudes 36.7°N–37.3°N (Fig. 1). Aftershock data are merged from the AFAD and KOERI (Bogazici University, Kandilli Observatory and Earthquake Research Institute). AFAD and KOERI provide the real time data with a great number of modern on-line and dial-up seismic stations in Turkey. Each station is equipped with a high-gain seismometer. The errors in hypocenter distribution are about 2–3 km depending on the allocation of the stations. These institutes compute the size of aftershock sequence of Bodrum-Kos earthquake with M_L. In this work, we did not relocate the aftershock epicenters and we used the aftershock epicenter locations provided by AFAD and KOERI.

The mainshock has a magnitude of $M_W = 6.5$ and $M_L = 6.2$ (with an intensity of Io = VII) and occurred at 22:31:9.7 UTC on July 21th, 2017. The earthquake is related to the south-striking Gökova Fault Zone (GFZ) and north-striking Datça fault (DF) which is dominated by normal faults (Kadirioğlu et al., 2017). According to the AFAD and KOERI records, Bodrum-Kos earthquake was followed by dense aftershock activity in a 6-month time interval from July 21th, 2017 to January 01, 2018. Fig. 2 shows the aftershock epicenters reported in the AFAD and KOERI catalogs and main tectonic structures of the surrounding area. Aftershock catalog is homogenous for local magnitude, M_L, and includes 10,600 aftershocks with magnitudes $0.2 \le M_L \le 5.1$. In order to make a detailed magnitude-time analysis, magnitude histogram and magnitude variations of aftershocks as a function of time are illustrated in Fig. 3. As shown in magnitude histogram given in Fig. 3a, aftershock sequence of Bodrum-Kos mainshock is completed between 1.0 and 3.0 magnitude bands. However, there are clear fluctuations in the number of aftershocks whose magnitudes change between 2.0 and 4.0, especially between 2.0 and 3.0 (Fig. 3b). There are 10,214 aftershocks with magnitude $M_L < 3.0$, 335 aftershocks $3.0 \le M_L < 4.0$, 50 aftershocks $4.0 \le M_L < 5.0$, and aftershock with

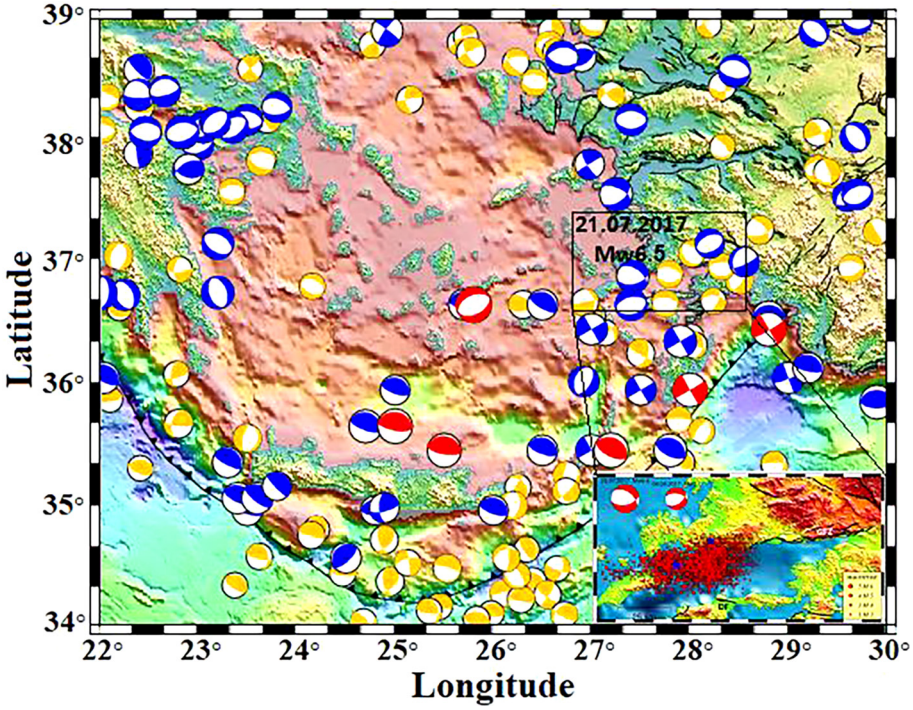

Fig. 1. Active tectonics in and around study region is between 27–28.5 E longitudes and 36.7–37.7 N latitudes plotted as rectangular area. The mainshock is marked as date and magnitude. Hellenic trench and active faults are shown by black line with the polarity of former subduction zones indicated by filled triangles and black lines respectively. Focal mechanism solutions are shown as red ball (magnitude 7Mw8), blue ball (magnitude 6Mw7) and yellow ball (magnitude 5Mw6). (For interpretation of the references to colour in this figure legend, the reader is referred to the web version of this article.)

$M_L = 5.1$ is the greatest of all (Fig. 2). Utsu and Seki (1954) investigated the relation between aftershock area and mainshock magnitude, and they introduced that the area is ellipse. Aftershocks, especially larger aftershocks, of 2017 Bodrum-Kos earthquake are generally distributed in an elliptical area and located between Kos-Bodrum-Çökertme-Gökova Gulf-Küçükgünlük Bay-Datça region in the east-west direction as seen in Fig. 2. The highest density of aftershocks (all size of shocks in general) is observed in all the parts of the mainshock epicenter whereas the larger events ($M_L \geq 4.0$), including the largest aftershock, are especially observed in the eastern part of the mainshock.

3.1. Preparation of aftershock data used in the analyses

In the analyses related to space-time-magnitude distribution of the aftershocks, especially in the estimation of *b* and *p*-value, the use of complete data set for all magnitude levels is quite important for reliable results in seismicity-based studies. For this reason, it is suggested to be used the maximum number of events. As one of the most important process, the minimum magnitude of completeness, *Mc*-value, based on the assumption of G-R power law distribution of magnitudes can be estimated. *Mc*-value can be theoretically described as the smallest magnitude that all the earthquakes are recorded. In other words, it can be defined as the minimum magnitude of complete reporting (Habermann, 1983; Mignan and Woessner, 2012). It means that *Mc* level contains 90% of the events which can be sampled with a power law fit (Wiemer and Wyss, 2000). *Mc*-value varies systematically in space and time according to different networks and catalogs. Therefore, temporal variations in this parameter can potentially cause incorrect *b* and *p*-value calculations. Because the network may be improved after the mainshock and during the first highest activity, small shocks may not be located since they fall within the coda of larger events. Thus, *Mc*-value will be higher in the early part of the aftershock sequence and this high value may produce incorrect estimations on statistical analyses (Wiemer and Katsumata, 1999). Temporal variations of *Mc*-value can

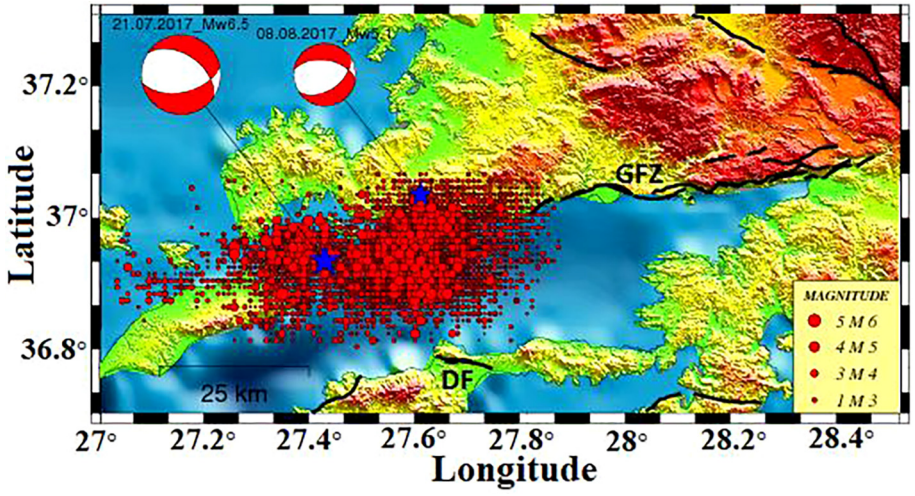

Fig. 2. Epicenter distribution of the aftershocks of Bodrum-Kos earthquake. Different magnitude sizes of the aftershocks are given by different symbols and mainshock epicenter with star (GFZ: Gökova Fault Zone and DF: Datça Fault).

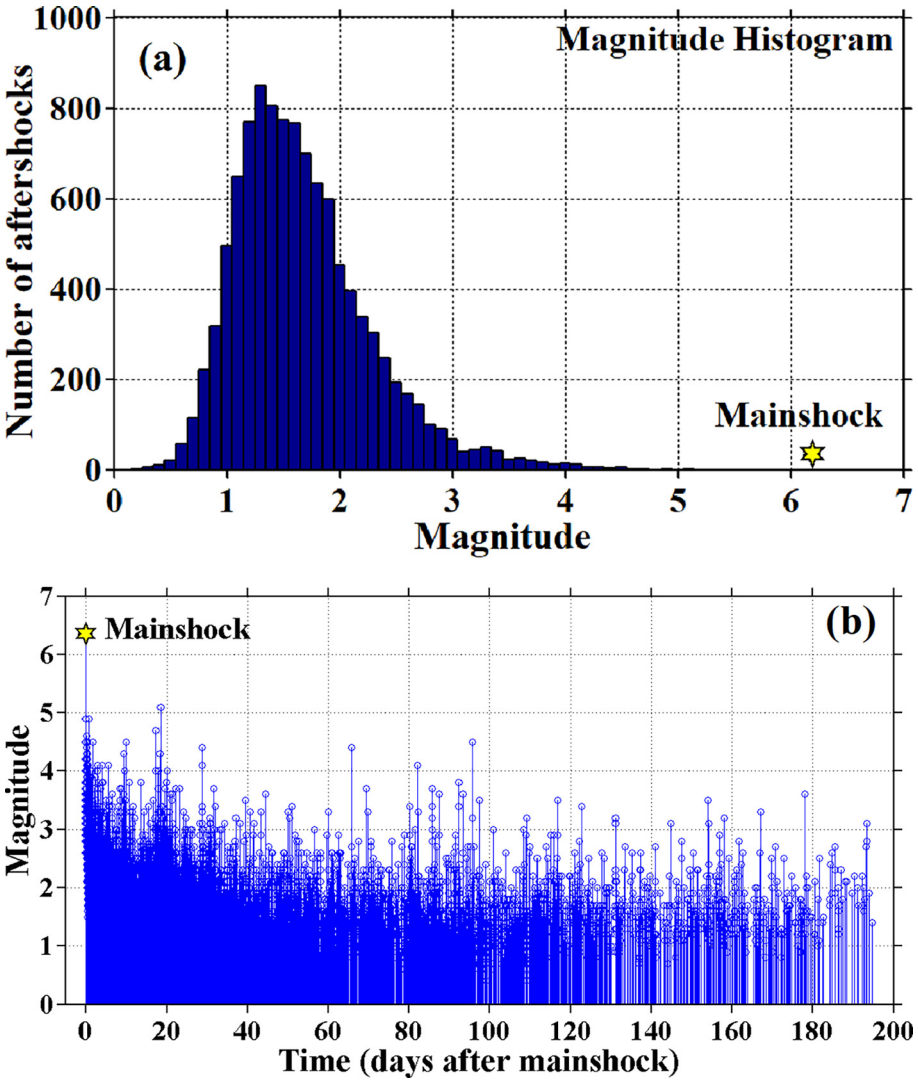

Fig. 3. (a) Magnitude histrogram of aftershock sequence, (b) magnitude variations of aftershock sequence as a function of time.

be estimated rapidly and safely by evaluating the goodness of fit to a power law. The variation of *Mc*-value as a function of time is provided by using a moving time window approach with the maximum likelihood method (for details see Wiemer and Wyss, 2000). For the aftershock sequence of Bodrum-Kos earthquake, we used an overlapping moving window technique (provided with ZMAP) to see the temporal change of *Mc*-value, starting at the mainshock time. We choose a sample window including 40 events in order to plot the temporal variations of *Mc*-value. Temporal change of *Mc*-value as a function of time is plotted in Fig. 4a. *Mc*-value is the largest at the beginning of the sequence (in the first ten hours) and varies from 2.5 to 3.1. Then, it shows a value between 1.5 and 2.5 after two days from the mainshock. *Mc*-value generally changes between 1.0 and 2.0, average $Mc = 1.5$, after 20 days from the mainshock. Therefore, we can say that *Mc*-value in the aftershock sequence does not show a stable value in time interval of six months. In order to understand how much *Mc*-value changes depending on the sample size, different sample sizes such as 25, 75 and 100 events/window were tested for aftershock sequence and it is concluded that the selection of the sample size does not affect the results. Thus, temporal fluctuations in *Mc*-value shown in Fig. 4a do not depend on the small sample size. In addition to temporal changes of *Mc*-value, spatial variation of *Mc*-value is also plotted in Fig. 4b. For the completeness map, we used a spatial grid of points with a grid of 0.01° in longitude and latitude. As can be seen from Fig. 4b, *Mc*-value changes between 1.1 and 2.2. *Mc*-value is mostly between 1.1 and 1.8 in the eastern and western parts of the aftershock area whereas it varies from 1.9 to 2.2 in and around mainshock epicenter. From this map, we can clearly see that seismic activity can be resolved to an *Mc*-value around 1.6 in most of the study region. Thus, *Mc*-value is selected as 1.6 in order to estimate the *b*-value.

In order to provide the completeness in the statistical analyses, two parameters must be arranged in the estimation of the decay parameters of aftershock sequence: (1) a minimum magnitude threshold *Mmin* and (2) a minimum time threshold *Tstart*, i.e. excluding the first hours to days from the analysis. *Mmin* can be selected for the shortest *Tstart* as the simplest approach. Therefore, this approach uses the largest *Mc*-value, which is defined for the earliest part of the aftershock sequence (Wiemer and Katsumata, 1999). However, this approach reduces the amount of available data by more than one order of magnitude. For Bodrum-Kos aftershock sequence, $Mmin = 2.3$ and $Tstart = 0.01$ were chosen to estimate the decay parameters of the modified Omori law. *c*-value is measured in time units, days for example. After some earthquakes, usually large ones, there is some delay (usually small) in the aftershock sequences. It can be noticed by just looking at the decay curve of aftershocks with time. In many cases, however, there can be a large incompleteness in the catalog at the very beginning of the aftershock sequence. Therefore, an artificial high *c*-value may be calculated. There is no upper limit of *c*-value. However, this value is usually small

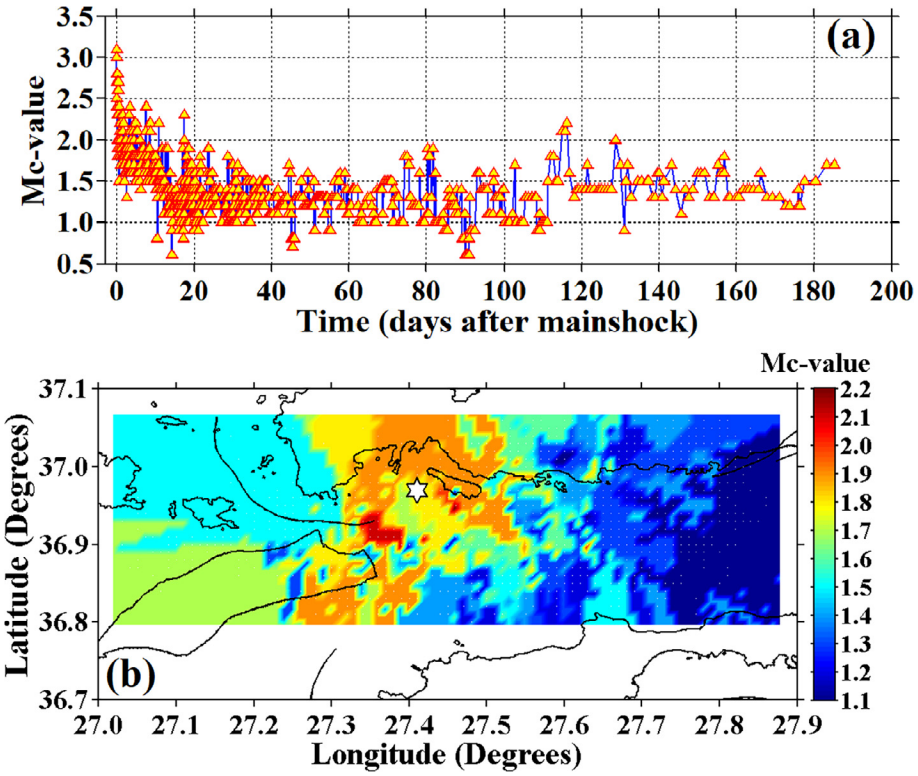

Fig. 4. (a) Temporal variations of magnitude completeness, *Mc*. *Mc*-value is estimated for overlapping temporal windows, containing 40 events, (b) spatial variation of *Mc*-value. Star indicates the mainshock.

or very small: for example, around 0.01. We aimed to remove these types of uncertainties on the calculations by taking *Mmin* = 2.3 and *Tstart* = 0.01 for the aftershock sequence. In this way, although the number of aftershocks is strongly reduced, the earliest part of the sequence is included in the analyses and we provided the completeness. As a result, for the estimation of decay parameters, we used 1614 aftershocks with magnitude equal to and larger than 2.3.

ZMAP software package (Wiemer, 2001) is used for all statistical estimations of aftershock parameters. The *b*-value in G-R relationship is computed by maximum likelihood method, because it yields a more robust estimate than least-square regression method (Aki, 1965). The parameters in the modified Omori formula are calculated accurately by the maximum likelihood method, assuming that the seismicity follows a non-stationary Poisson process (Ogata, 1983). *Dc*-value for aftershock sequence is estimated in 95% confidence limits by least squares method (Nanjo et al., 1998). A gridding technique is used for spatial mapping of the frequency-magnitude distribution and the decay rate of the aftershocks, and we considered the nearest epicenters, *Ne*, for each node of the grid (Wiemer and Wyss, 1997; Wiemer and Katsumata, 1999). The algorithm (Wiemer and Wyss, 2000) determines the minimum threshold magnitude for which the goodness of fit is greater than or equal to 95%. If there is no such magnitude for the given confidence level, a 90% goodness of fit is assigned instead. If, however, the goodness of fit is less than 90% for any threshold magnitude, the magnitude where the frequency-magnitude distribution has its maximum curvature is determined. One of these magnitudes assigns as *Mc*-value for that grid point. If the number of aftershocks with $M \geq Mc$ is equal to or greater than the minimum number of the nearest epicenters, *Nemin*, *b* and *p*-values are calculated for that node by using only the aftershocks with $M \geq Mc$. Then, spatial mapping of *b* and *p*-values are plotted by the ZMAP software.

4. Assessing the seismotectonic parameters of aftershock sequence

In this study, a statistical evaluation of aftershock sequence of July 21th, 2017 Bodrum-Kos earthquake was made by analyzing the distribution in space-time-magnitude distribution. For this purpose, several seismotectonic parameters related to aftershock hazard assessment were investigated. Variations in the cumulative number of aftershocks in six months after the Bodrum-Kos mainshock are plotted in Fig. 5a. If we consider the aftershock activity from the mainshock time to six months in which many aftershocks are recorded, Fig. 5a can be divided into two subregions. The first month can be considered as the first region and the following five months as the second region. There are 6946 aftershocks in the first month after the mainshock whereas 1676 events are recorded in the second month, 884 events in the third month, 585 events in the fourth month, 266 events in the fifth month and 243 events in the last month. Aftershock activity after the second month from the mainshock is relatively more stable and shows a more rapid decrease in comparison with the activity of the first two months. These variations in the number of aftershocks in six months are also clearly seen in Fig. 5b. As seen in time histogram of the aftershocks given in 5b, aftershock activity in the first 30 days shows more densely distribution whereas it shows a more stable distribution after the first 40 days from the mainshock. Then, average number of aftershocks decrease with time according to the modified Omori law (hyperbola on Fig. 5b). We can obviously see from Fig. 5b that aftershock activity come to end after six months. Tajima and Kanamori (1985) stated that aftershocks of large earthquakes may continue a year. Also, if a shock occurs in 100 or 150 days after the mainshock, it can be considered as an aftershock (Tsapanos et al., 1994). Many authors used different time intervals changing between one and six months for different aftershock sequences; for example, four months in Enescu and Ito (2002), five months in Bayrak and Öztürk (2004), one month in Öztürk et al. (2008), six months in Nuannin et al. (2012) and in Ansari (2017).

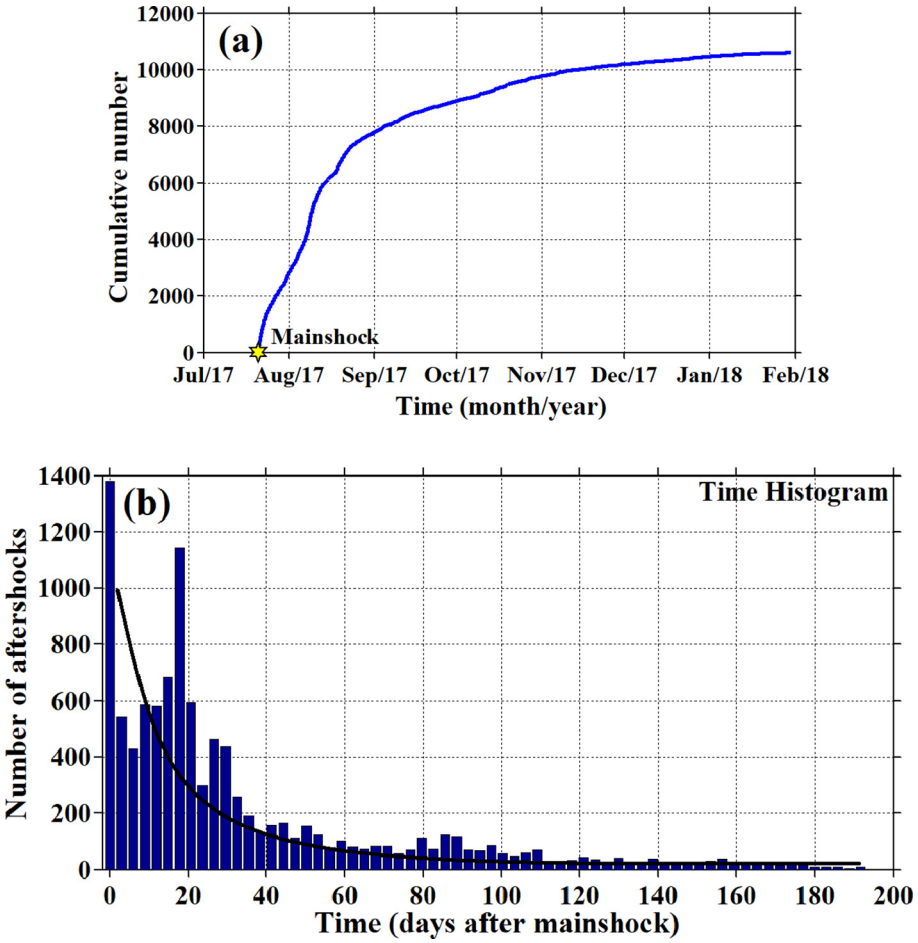

Fig. 5. (a) Cumulative number of aftershock in six months after the mainshock, (b) changes in the number of aftershocks as a function of time after the mainshock. Black hyperbola indicates the least squares fixed the modified Omori law.

Considering these assessments and aftershock activity in study region, we used the aftershock activity in a 6-month time interval for July 21th, 2017 Bodrum-Kos earthquake.

Cumulative magnitude-frequency of Bodrum-Kos aftershock sequence is shown in Fig. 6a. For the *b*-value estimation of frequency-magnitude relation of the aftershock sequence, *Mc*-value is taken as 1.6, based on the goodness of fit of the aftershock data. We used this *Mc*-value considering the temporal variations given in Fig. 4a. *b*-value and its standard deviation, as well as the *a*-value of G-R relation, were calculated with the maximum likelihood method. For the aftershock sequence, *b*-value is estimated as 0.90 ± 0.05 with this *Mc* value. At the first sight, this *b*-value can be considered as relatively small but obtained *b*-value for aftershock sequence is close to 1.0. As a result, aftershock sequence matches the general feature of aftershocks such that magnitude-frequency distribution of aftershocks is represented by the G-R law with a *b*-value typically close to 1 (Frohlich and Davis, 1993). As stated in Frohlich and Davis (1993), smaller *b*-value may be related to the low heterogeneity degree of medium, the higher stress concentration or high strain in the earthquake region. A detailed assessment of the dependence of *b*-value on the interval size, maximum magnitude, sample size and the data fitting techniques was carried out by Bender (1983). Also, *b*-value is mostly used to explain the relative number of small and large magnitude earthquakes. A small *b*-value shows a large proportion of high magnitude events or *b*-values may show slight increases when a larger magnitude levels were not included in the estimations. As stated in the data section, there are 335 aftershocks with magnitude $3.0 \leq M_L < 4.0$ and 51 aftershocks with magnitude $M_L \geq 4.0$. Thus, this relatively small *b*-value may be caused by relatively abundance of aftershocks having larger magnitude with $M_L \geq 4.0$. Temporal change in *b*-value for the Bodrum-Kos aftershock sequence is computed for six month intervals and shown in Fig. 6b. For the variation of *b*-value as a function of time, moving window approach and the maximum likelihood method are used. A sample size of 350 events is preferred in the estimation of temporal *b*-value. As can be seen in Fig. 6b, b-values change in a narrow band from 0.7 to 1.0. *b*-values show some important increases and decreases over the time after the mainshock. Arrows on Fig. 6b show the occurrence times with their magnitudes of the largest three aftershocks after the mainshock. From Fig. 6b, one can clearly see that sudden decreases in *b*-value coincide with the occurrence times of the larger aftershocks whereas the rapid increases are observed after the occurrences of the larger aftershocks. However, *b*-value changes around an average value of 0.9. As stated in many studies, there are several factors which can cause perturbations of the normal *b*-value. The applied shear stress may increase after the mainshocks, which would be compatible with low *b*-values. Therefore, we can interpret that decreasing anomalies in temporal *b*-value before the occurrence times of larger aftershocks may be due to a stepwise increase in effective stress. Also, sudden increase in temporal *b*-value may be related with the reduced stress in these times after the large aftershocks. As a result, the evaluation of temporal variations in magnitude-frequency distribution may have a statistical significance for aftershock hazard assessment after a mainshock.

Fig. 7 shows the decay rate of aftershock activity versus time after the mainshock for aftershocks with magnitude $Mc \geq Mmin$ for the Bodrum-Kos aftershock sequence. In order to estimate the *p*, *c* and *K*-values, the maximum likelihood procedure was used, and the

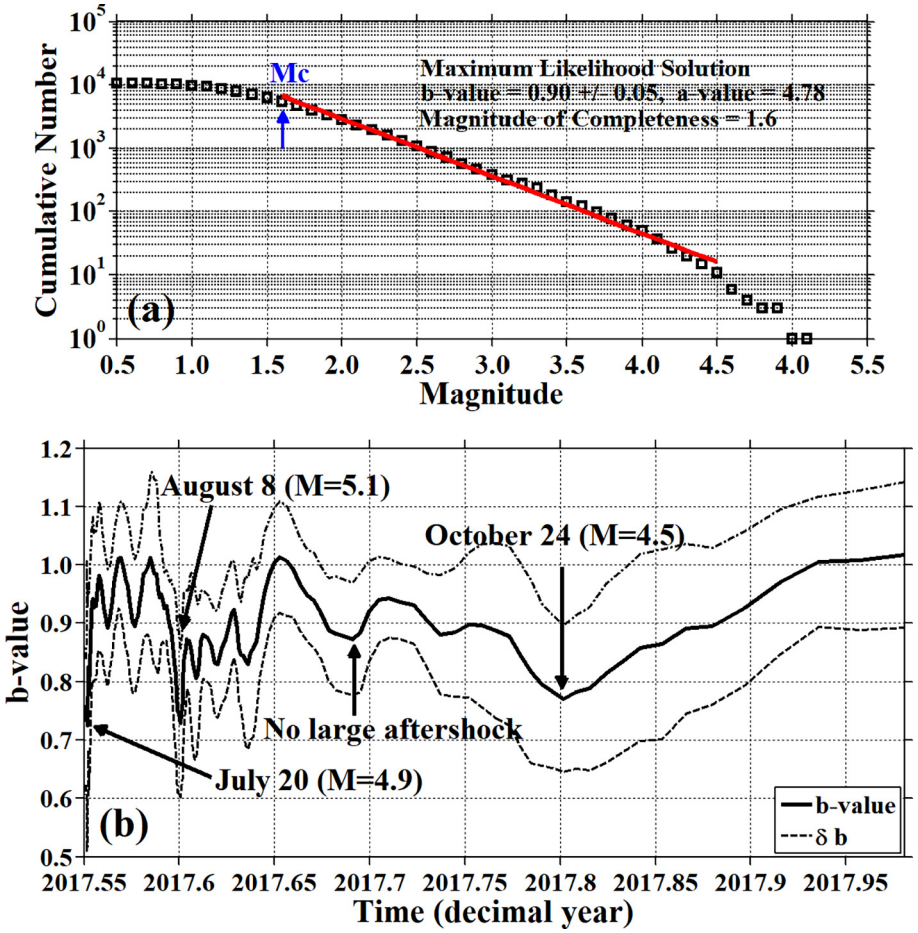

Fig. 6. (a) Gutenberg-Richter relation of aftershock sequence. *b*-value, its standard deviation, *Mc*-value as well as the *a*-value in the Gutenberg-Richter relation are given, (b) Temporal changes in *b*-value. Arrows indicate the decreases in *b*-value before the occurrences of large aftershocks.

aftershock occurrence was modeled by the modified Omori model. $p = 1.04 \pm 0.02$, nearly close to the global *p*-value 1, is calculated for the sequence assuming to be *Mmin* = 2.3, *Tstart* = 0.01. *c*-value is 0.224 ± 0.039. As suggested in Helmstetter and Shaw (2006) and Peng et al. (2007), since the great *p*-value may be caused from the high stress heterogeneity, we can conclude that there is not stress heterogeneity in the Bodrum-Kos aftershock sequence. Large *p*-value for a given aftershock sequence also indicates a fastest decay of aftershock activity and thus, the occurrence of aftershocks in the Bodrum-Kos earthquake shows a relatively fast decay rate. Utsu et al. (1995) stated that the superposed sequences include usually small sized aftershocks and a portion of these events may not be real aftershocks; they may only

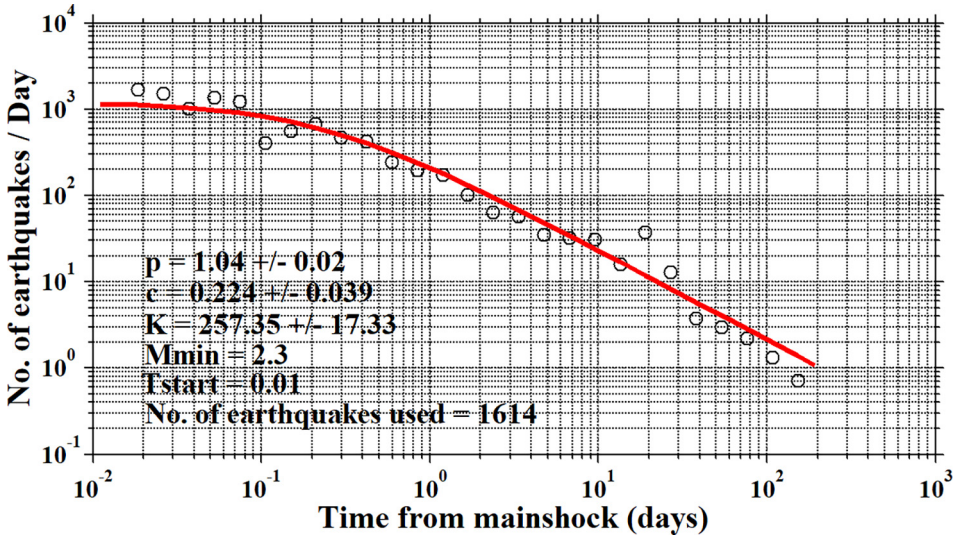

Fig. 7. Modified Omori model and decay parameters aftershock activity of Bodrum-Kos (for the cases: $M_L \geq 2.3$). Aftershock parameters such *p, c* and *K*-values in the modified Omori formula, the minimum magnitude, starting time for the data and the number of aftershocks are also given.

Table 1
Detailed statistics for the estimation of aftershock decay parameters.

No	*Tstart* (days)	*Mmin*	Time interval (*t*, days)	Number of aftershocks used	*p*-value	*c*-value	*K*-value
1	0.05	1.6	$0.05 \le t \le 193.8667$	5444	1.63 ± 0.05	8.677 ± 0.740	15488.83 ± 3280.53
2	0.05	2.1	$0.05 \le t \le 193.2306$	2293	1.14 ± 0.03	0.882 ± 0.124	604.2 ± 56.79
3	0.05	2.2	$0.05 \le t \le 193.2306$	1899	1.09 ± 0.03	0.540 ± 0.088	404.39 ± 37.40
4	0.05	2.3	$0.05 \le t \le 193.2306$	1561	1.07 ± 0.02	0.326 ± 0.063	285.86 ± 22.90
5	0.1	1.6	$0.10139 \le t \le 193.8667$	5389	1.68 ± 0.05	9.697 ± 0.840	19681.46 ± 4564.69
6	0.1	2.1	$0.10139 \le t \le 193.2306$	2238	1.19 ± 0.03	1.285 ± 0.182	749.60 ± 85.12
7	0.1	2.2	$0.10139 \le t \le 193.2306$	1844	1.15 ± 0.03	0.852 ± 0.140	494.54 ± 52.32
8	0.1	2.3	$0.10139 \le t \le 193.2306$	1506	1.11 ± 0.03	0.558 ± 0.108	343.50 ± 34.54
9	0.01	1.6	$0.01111 \le t \le 193.8667$	5497	1.58 ± 0.04	7.652 ± 0.644	12057.95 ± 2315.03
10	0.01	2.1	$0.01111 \le t \le 193.2306$	2346	1.10 ± 0.02	0.621 ± 0.085	511.41 ± 40.55
11	0.01	2.2	$0.01111 \le t \le 193.2306$	1952	1.06 ± 0.02	0.367 ± 0.057	351.95 ± 25.31
12	0.01	2.3	$0.01111 \le t \le 193.2306$	1641	1.04 ± 0.02	0.224 ± 0.039	257.35 ± 17.33
13	–	2.1	$0.020833 \le t \le 193.2306$	2361	1.09 ± 0.02	0.560 ± 0.076	489.43 ± 36.98
14	–	2.2	$0.020833 \le t \le 193.2306$	1967	1.05 ± 0.02	0.330 ± 0.050	340.11 ± 23.31
15	–	2.3	$0.020833 \le t \le 193.2306$	1629	1.03 ± 0.02	0.204 ± 0.035	251.31 ± 16.17
16	–	2.4	$0.020833 \le t \le 193.2306$	1326	1.01 ± 0.02	0.124 ± 0.024	184.54 ± 11.37
17	–	2.5	$0.020833 \le t \le 193.2306$	1078	1.00 ± 0.02	0.078 ± 0.017	138.97 ± 8.41
18	–	2.6	$0.020833 \le t \le 193.2306$	886	1.00 ± 0.03	0.055 ± 0.013	108.88 ± 6.65
19	–	2.7	$0.020833 \le t \le 193.2306$	718	1.01 ± 0.02	0.039 ± 0.011	85.64 ± 5.35
20	–	2.8	$0.020833 \le t \le 193.2306$	575	1.01 ± 0.02	0.030 ± 0.009	66.61 ± 4.37
21	–	2.9	$0.020833 \le t \le 193.2278$	476	1.00 ± 0.03	0.021 ± 0.007	52.53 ± 3.58
22	–	3.0	$0.020833 \le t \le 193.2278$	386	1.01 ± 0.03	0.016 ± 0.006	41.83 ± 3.01
23	–	3.1	$0.020833 \le t \le 193.2278$	318	1.02 ± 0.03	0.014 ± 0.006	34.23 ± 2.65
24	–	3.2	$0.020833 \le t \le 178.0833$	279	1.04 ± 0.03	0.018 ± 0.008	31.29 ± 2.64
25	–	3.3	$0.020833 \le t \le 178.0833$	236	1.06 ± 0.04	0.021 ± 0.009	27.13 ± 2.52

represent background seismicity. As stated in Data section, Bodrum-Kos aftershock sequence has 10,214 events whose magnitudes are smaller than 3.0. Also, the catalog consisting of the first month has 6946 aftershocks. In order to test the confidence of the results for *p* and *c*-values for the aftershock sequence, we considered the effects of different *Mmin* and *Tstart*. All estimations are given in Table 1. Utsu et al. (1995) pointed out that the *p*-value is independent of *Mmin*, but the *c*-value depends heavily on the *Mmin* of the data. We made several tests to our parameters for different *Mmin* (ranging from 1.3 to 3.3) and *Tstart* values (ranging from 0.002 to 0.1). Thus, we saw that the *p*-value varies from 1.00 to 1.68 for different *Mmin* and *Tstart* but *c*-value changes between 0.014 and 9.697. In fact, *c*-value is suggested to strongly related to the minimum magnitude in comparison with *p*-value.

A number of statistical techniques have been applied to model the decay rate of aftershocks and to describe the behaviors of aftershock sequences as a power law since the first description by Omori (1894). Although alternative models such as Epidemic Type Aftershock Sequence (ETAS) model (Ogata, 1983), Marcellini (1997) approach, stretched exponential relaxation (Mignan, 2015), modified Omori law including a background rate term (Öztürk et al., 2008), etc., have been suggested to map the aftershock decay rate, different models have limited results relative to the modified Omori law. Among different models, the modified Omori law is one of the most effective approaches, and aftershock time series analyzed in this study are all well fit with the modified Omori model. Hence, and also considering the detailed statistics given in Table 1 (as seen in test 12), the modified Omori law seems suitable to model the decay rate of Bodrum-Kos aftershock sequence.

The number of aftershocks may not be counted completely at the beginning of a sequence when smaller events are often hidden by greater ones due to overlapping, thus too large *c*-value is obtained. Utsu (1971) stated that *c*-value may be zero if all events can be counted. There are two ideas in relation to *c*-value: one is that *c*-value is actually 0 and all the reported positive *c*-values result from incompleteness in the early stage of an aftershock sequence. The second opinion is that positive *c*-value can be obtained (Enescu and Ito, 2002). If $c = 0$, $n\,(t)$ in Equation (2) diverges at $t = 0$. If the enlargement of the aftershock region occurs in an early stage, a relatively large *c*-value may be calculated (Utsu et al., 1995). Also, for the aftershock sequences following relatively small mainshocks, estimated *c*-values are generally small ($c \le 0.01$ days). Hirata (1969) stated that *c*-value changes between 0.02 and 0.5 for the 1969 Shikotan-Oki earthquake (*M*6.9; from Utsu, 1969). Considering these detailed literature studies, we can conclude that the use of *Mmin* = 2.3 and *Tstart* = 0.01 for the estimation of decay parameters seems better to fit the Bodrum-Kos aftershock sequence. These results are in accordance with other studies and also suggest that aftershock activity does not have a heterogeneous background seismicity pattern. Thus, the simple modified Omori model appears suitable to describe the aftershock decay parameters in Bodrum-Kos earthquake sequence.

Fig. 8 shows the fractal dimension of aftershock epicenter distributions for Bodrum-Kos earthquake. *Dc*-value is estimated by fitting a straight line to the curve of mean correlation integral versus the event distance, *R* (km), as seen in Fig. 8. *Dc*-value is calculated as 1.74 ± 0.09 for epicenter distribution of 10,600 aftershocks with 95% confidents interval by the least squares method. This log-log relation displays a clear linear range and scale invariance in the self-similarity statistics between 4.66 and 24.91 km (indicated in Fig. 8 as "Range"). In the selection of the minimum size range (*Rmin*) for the estimation of *Dc*-value, the epicentral error size is taken into account and the selection of this parameter is important. Epicentral errors changes as regionally and depending on the time for different parts of Turkey. But, this variation is generally between 5 and 10 km in space and time for the epicenters of Turkey earthquakes. Kagan and Knopoff (1980) stated that the minimum size range (*Rmin*) is related to the epicentral error sizes of earthquakes in the study region or the error in epicentral sizes whereas the maximum size range (*Rmax*) is related to the size of study region. Fractal statistical interval was given between 5 and 160 km by Öncel et al. (1996) for different parts of the North Anatolian fault Zone, between 3.6 and 70 km by Polat et al. (2008) for Aegean Extension region. Thus, the minimum size range (*Rmin* = 4.66 km) used in the estimation of *Dc*-value in this study is consistent with literature. As mentioned above, fractal analysis based on the correlation integral may be used to evaluate the spatial features of the aftershock occurrence (Yadav et al., 2011, 2012). Fractal dimension may also be used as a quantitative measure of heterogeneity degrees in fault geometry and stress (Ansari, 2017). If there is an increasing complexity in the active fault system

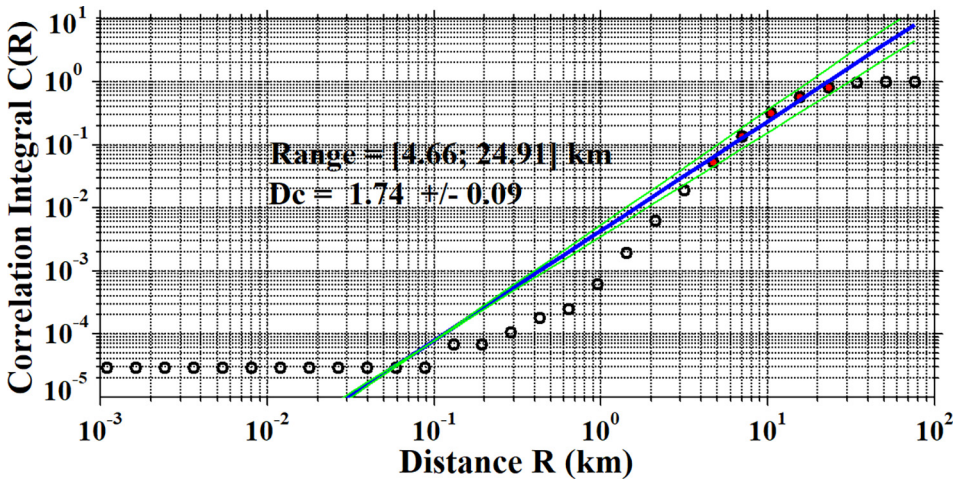

Fig. 8. Fractal dimension, *Dc*-value, for Bodrum-Kos aftershock sequence.

with higher *Dc*-value and smaller *b*-value, the stress release occurs on fault planes of smaller surface area (Öncel and Wilson, 2002). Also, the larger *Dc*-value is sensitive to heterogeneity in magnitude distribution. *Dc*-value calculated as 1.74 ± 0.09 in this study suggests that aftershocks are more clustered at larger scales or (in smaller areas) and this large *Dc*-value may be a dominant structural characteristic for aftershock region. Since *Dc*-value is close to 2.0, we can imply that Bodrum-Kos aftershocks are homogeneously distributed. Also, heterogeneity degree of seismicity can be evaluated quantitatively with the fractal dimension, and the heterogeneity of stress field controls the region (Öncel et al., 1996). Hence, it can be obtained a non-heterogeneous stress distribution in Bodrum-Kos region. Thus, we can statistically describe and characterize the spatial distributions of aftershock epicenters and their fracture systems with fractal dimension.

5. Regional changes in *b*-value, *p*-value and the maximum aftershock magnitudes

For the regional images of *b*-value and *p*-value, we used the procedure in which is described at the end of Section 3.1. A spatial grid of points having a nodal separation of 0.01° (about 1.1 km) in latitude and longitude was used. Then, we considered the closet nearest epicenters (number of events, *Ne*) as 350 aftershocks for each node and the minimum nearest epicenters (minimum number of events > *Mc*), *Nemin*, was considered as 100 aftershocks. Next, the spatial images of *b*-value and *p*-value were plotted by using between 100 and 350 aftershocks, and these parameters were represented by using a color node on the maps. A significant acceptance is that *c*-value was selected as 0.224 days and so *Tstart* = 0.01 days for the estimation of *p*-value in the modified Omori formula since these assumptions are more satisfying (as seen in Table 1) to plot the spatial variations. Since spatial and temporal changes in *Mc*-value as plotted in Fig. 4a and b show changes between 1.1 and 2.2, *Mc*-value may be considered as around 1.6 for most of the nodes. Then, this minimum threshold magnitude is selected by ZMAP as *Mc*-value for all grid point. If the number of aftershocks with $M \geq Mc$ is equal to or greater than *Nemin* in each grid, *b*-value and *p*-value are estimated for that node by using only the aftershocks with $M \geq Mc$, otherwise, regional images of *b*-value and *p*-value cannot be created. Both the regional maps of *b*-value and *p*-value were created by using the same grid and number of aftershocks in each grid node, and the maximum likelihood method was used in the estimation of these two parameters. Thus, spatial variations of *b*-value and *p*-value were plotted by using *Ne* = 350 with *Nemin* = 100 aftershock for Bodrum-Kos sequence.

Figs. 9a and 10a show the regional changes in *b*-value and *p*-value for Bodrum-Kos aftershock sequence, respectively. Regional changes in *b*-value vary from 0.5 to 1.2, and *p*-value shows a distribution between 0.4 and 1.3. Regional variations of the standard deviation of *b*-value were plotted in Fig. 9b and it changes between 0.02 and 0.10, most of which less than 0.07. Also, regional distributions of the standard error in *p*-value were shown in Fig. 10b and it changes between 0.03 and 0.08, most of which less than 0.05. Considering the change interval in *b*-value, *p*-value and their standard errors according to several researchers such as Utsu (1971), Olsson (1999), Enescu and Ito (2002), Öztürk et al. (2008), Enescu et al. (2011), Ansari (2017) etc., a general conclusion is that *b*-value and *p*-value variations as well as their standard deviations for Bodrum-Kos aftershock sequence are accordance with these results. Aftershock activity of Bodrum-Kos sequence is densely distributed in the eastern part of mainshock epicenter. The larger aftershocks ($3.0 \leq M_L < 4.0$) are recorded in and around the mainshock epicenter (as seen in Figs. 1 and 2), and from the mainshock epicenter to the east, west, south, southeast and southwest directions. Also, the larger aftershocks whose magnitude changes between 4.0 and 5.0 show an intense distribution from the mainshock epicenter to the east, west, southeast and southwest directions. We can divide the *b*-values into three groups: (1) the lowest *b*-values (< 0.8) to the west, north, northwest and southeast parts of the mainshock (in and around mainshock, including Karaada, Bodrum, Akyarlar and Turgutreis), (2) intermediate *b*-values (around 1.0) to the southwest direction from the mainshock epicenter (in and around Kos island), and (3) the largest *b*-values (> 1.1) to the northeast part of the mainshock (including Çökertme, Bozalan, Fesleğen, Gökpınar and Ören). Lower *b*-values are generally observed in the larger aftershock ($M_L \geq 4.0$) areas whereas the largest *b*-values are related to the area in which small shocks ($M_L < 3.0$) generally occurred. The *p*-values for Bodrum-Kos aftershock sequence show both small and large changes in all the study region. The largest *p*-values (> 1.0) are found in the north, south and southeastern parts of the mainshock epicenter (including Bodrum, Karaada, Bitez, Konacık and Gürece), and the activity in these parts shows the fastest decay of aftershock activity. Conversely, the lower *p*-values (< 0.7) regions are observed related to the eastern and western ends of the study area including the northwest part of Kos island and Gökova Gulf (Çökertme, Bozalan and Ören). This result gives the appearance that decay is slower than the other parts at these ends of the region. Consequently, aftershock activity decays in the eastern and western ends of the sequence ($p \sim 0.5$) much slower than that of along the north, south and southeastern parts.

As an another step of this study, we aimed to estimate the maximum magnitudes of aftershocks (Mamax) in Bodrum-Kos earthquake sequence. Båth (1965) suggested that average difference between mainshock magnitude and the largest aftershock magnitude is constant and equal to 1.2. For Turkey earthquakes, however, Öztürk (2009)

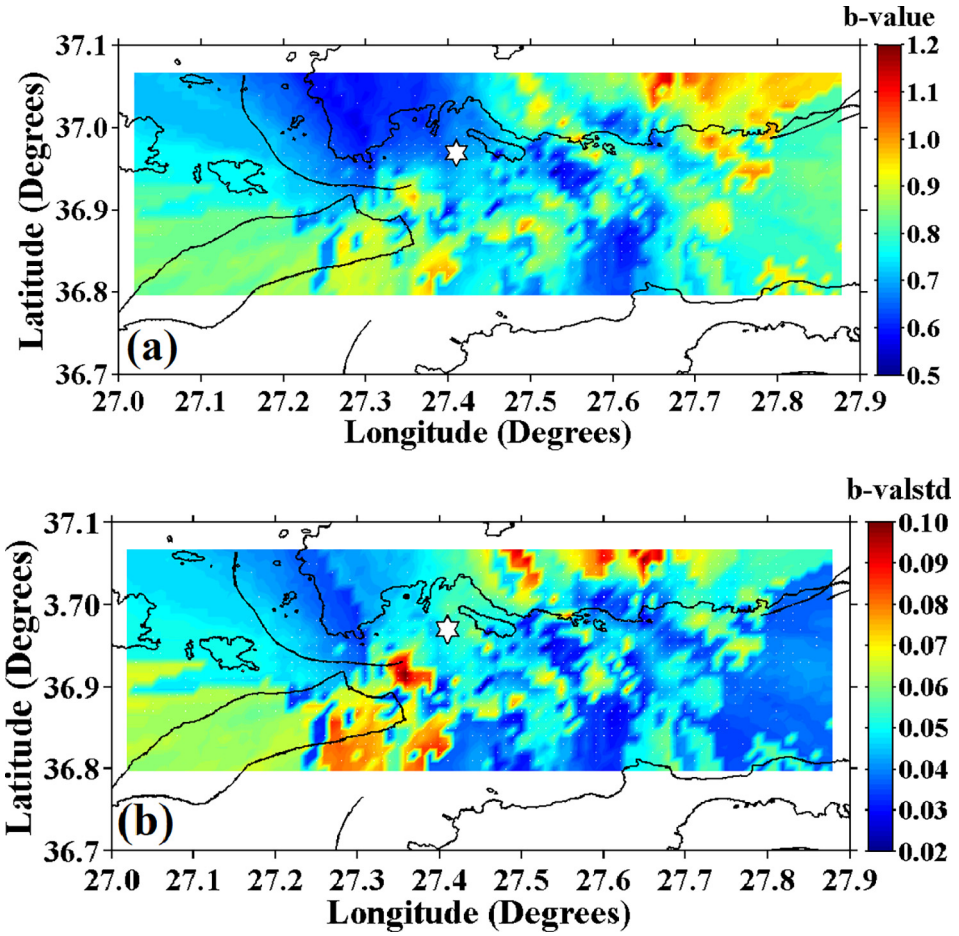

Fig. 9. (a) Spatial distribution of *b*-value (b) spatial distribution of standard errors in *b*-value. *b*-value and its standard deviation are determined by sampling the nearest 350 aftershocks for each node of a grid with nodal separation of 0.01°. Star indicates the mainshock.

calculated this difference as 0.9 from G-R relationship. Öztürk (2009) used eleven aftershock sequences and developed some relationships among different aftershock parameters such as the number of aftershocks, the magnitude of the largest aftershocks, *b*-value, *p*-value versus the mainshock magnitude, etc. Also, the difference between the main hock and the largest aftershock magnitude was estimated as 0.9 from G-R relationship. Some details on parameter values of aftershock sequences used by Öztürk (2009) are given in Table 2. According to the results in Öztürk (2009), the difference between the mainshock magnitude and the largest aftershock magnitude changes between 0.6 and 2.0 depending on the original catalog, and between 0 and 1.5 from G-R relationship. In order to evaluate the changes of possible maximum magnitudes in the aftershock sequence, spatial variation of maximum aftershock magnitudes for Bodrum-Kos earthquake sequence are plotted in Fig. 11. Spatial distribution of Mamax varies from 3.0 to 5.2. The larger Mamax values (> 4.4) were estimated in the west, north, northwest, northeast and southeast parts of the mainshock (in and around mainshock, including Bodrum and Akyarlar) whereas smaller Mamax values (< 3.6) were observed from the south direction of the mainshock and eastern end of the study region. When compared with the *b*-value spatial distribution, one can see clearly a relation between *b*-values and maximum aftershock magnitudes. Chung-Han and Yih-Min (2013) made a study on the maximum magnitudes in aftershock sequences in Taiwan and suggested that, once a database for the regional variations of *b*-values has been defined, the corresponding maximum aftershock magnitude can be estimated immediately following the mainshock occurrence. Chung-Han and Yih-Min (2013) is also stated that this type of analysis can give useful clues in order to reduce seismic hazard since a fast assessment of the short-term earthquake hazard shortly after a strong earthquake may supply information on destruction evaluations or urgent intervention. Therefore, this type of estimation can be implemented in order to forecast the next occurrence of a strong aftershock. Thus, a special interest needs to be given to these regions where Mamax value was observed.

6. Discussion on regional variations of *b*-value and *p*-value

Regional changes in *b*-value and *p*-value for an aftershock sequence can be used in order to make an evaluation on materiel properties and rupture mechanisms of an aftershock region. As stated in different past studies mentioned above, there is a clear relation between these aftershock parameters and the tectonic condition of the aftershock region such as stress and slip distribution, surface heat flow and structural heterogeneity. Temporal properties of 39 aftershocks occurrence in southern California were analyzed by Kisslinger and Jones (1991) and they could not find any relation of *p* with either *b*-value of the sequence or the mainshock magnitude. Their results show that *p*-values changes between 0.688 and 1.809 and they propose a direct relationship between *p*-value and surface heat flow. They suggested that shortened stress relaxation times in the fault zone materials causes higher temperatures in the aftershock source zone and leads to a larger *p*-value. Wiemer and Katsumata (1999) evaluated the spatial distribution of *b*-value and *p*-value for the Landers, Northridge, Morgan Hill and Kobe aftershock sequences. They suggested that spatial variability of *b* and *p*-values is related to the slip distribution during the mainshock, and the largest slip regions is correlated with large *b*-value. They supposed that the frictional heat formed during the mainshock may have an influence on the *p*-value changes of the aftershock region whereas *b*-value

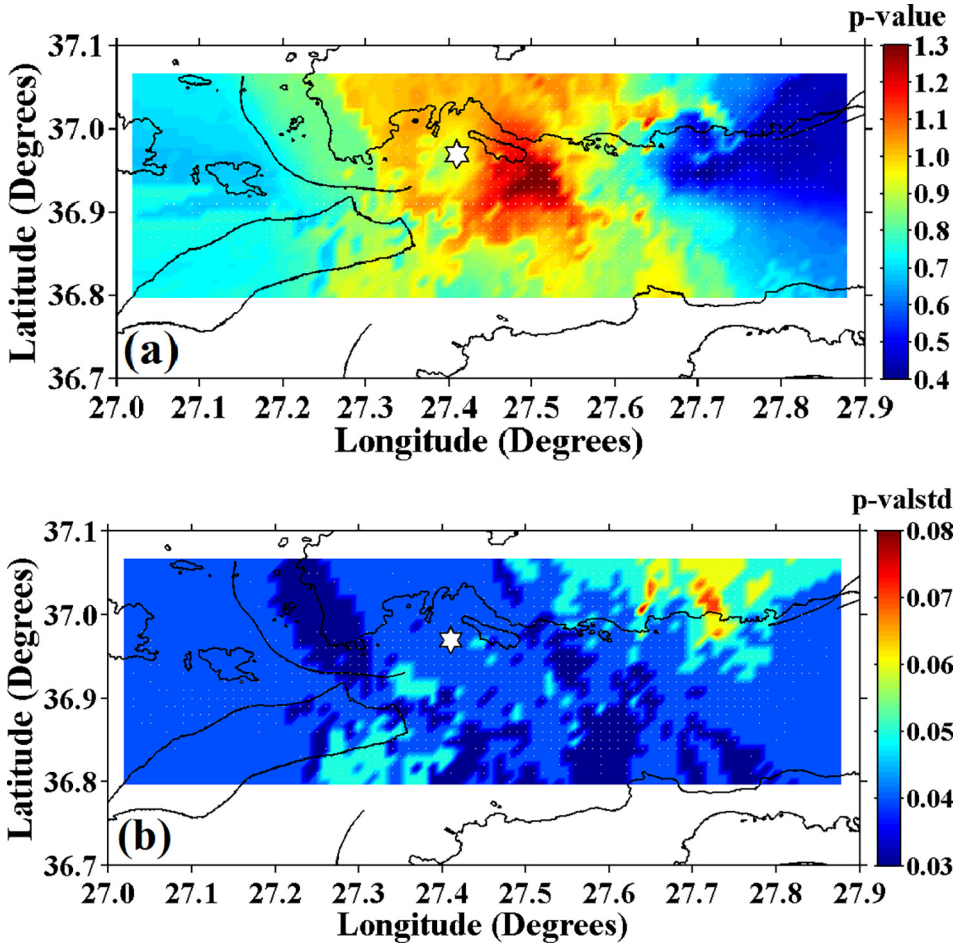

Fig. 10. (a) Spatial distribution of *p*-value, (b) spatial distribution of standard errors in *p*-value. *p*-value and its standard deviation are determined by using the same grid and number of aftershocks in each grid node as in the case of *b*-value map.

Table 2
Some parameter values of eleven aftershock sequences (from Öztürk, 2009).

Earthquake	Magnitude (M_d)	(Mamax)	Δm	Mamax*	Δm*
27 January 2003, Tunceli	6.2	4.2	2.0	4.80	1.40
1 May 2003, Bingöl	6.4	4.6	1.8	4.90	1.50
13 July 2003, Malatya	5.3	4.5	0.8	4.70	0.60
28 March 2004, Erzurum	5.3	4.6	0.7	5.30	0.00
11 August 2004, Elazığ	5.3	4.5	0.8	4.55	0.75
25 January 2005, Hakkari	5.4	4.6	0.8	5.15	0.25
12 March 2005, Bingöl	5.6	4.3	1.3	4.10	1.50
14 March 2005, Bingöl	5.9	4.7	1.2	4.55	1.35
23 March 2005, Bingöl	5.4	4.8	0.6	4.55	0.85
6 June 2005, Bingöl	5.1	4.3	0.8	4.20	0.90
26 November 2005, Malatya	5.1	4.2	0.9	4.40	0.70

M_d: Mainshock magnitude (duration magnitude), Mamax: the largest aftershock magnitude from original catalog, Δm: M_d-Mamax, Mamax*: the largest aftershock magnitude from G-R relationship, Δm*: M_d – Mamax*.

variations are related to stress changes, pore pressure and crack density. They also stated that both *b*-value and *p*-value are used in the aftershock probability evaluation, and regional changes of these parameters have an important influence on aftershock hazard assessments. Enescu and Ito (2002), Bayrak and Öztürk (2004), and Öztürk et al. (2008) made detailed statistical analyses for the spatial and temporal variations of the frequency-magnitude distribution and decay rate of different aftershock sequences from Japan and Turkey. They all suggested that there is a general relationship among the regional variations of *b*-value and *p*-value, the rupture mechanism and material properties of an aftershock region. They suggested that smaller *b*-value changes are related to lower stress distribution after the mainshock and larger *p*-values correlate with the regions that experienced higher slip during mainshock. The results of these studies may be summarized in two points: (*i*) the regional variations of *b*-value and *p*-value is controlled by rupture mechanisms during mainshock, (*ii*) changes in these variables depends on the material properties of the aftershock region. In addition to these studies, in recent years, many researchers such as Enescu et al. (2011), Nuannin et al. (2012), Zhang et al. (2013), Nemati (2014), Ávila-Barrientos et al. (2015), Hainzl et al. (2016), Wei-Jin and Jian (2017), Ansari (2017) made valuable investigations which are focused on these types of aftershock assessments, especially on *b*-value and *p*-value analyses for different aftershock sequences. General conclusions on *b*-value and *p*-value from these studies may be summarized as (*i*) spatial and temporal variations in these parameters have a good relation to the crustal structure and/or some parameters of the earthquake process, (*ii*) the most determinative factor controlling the spatial variations on these variables is probably the fault slip, (*iii*) spatial and temporal changes in these parameters are statistically significant and hold significant information for practical forecast, (*iv*) the effects of aftershock sequences may be used in order to evaluate the nonlinear seismic response and accumulated damage of concrete gravity dams, (*v*) spatial assessments of the aftershock sequence correspond quite well to the causative fault planes of earthquakes, (*vi*) apparent trend in these parameters is a reflection of the tendency of the plate to increase in age (and thus in thermal features) at the subduction zone, so tectonic structure may control the aftershock generation, (*vii*) analyses of aftershock sequences may benefit for earthquake hazards mitigation in

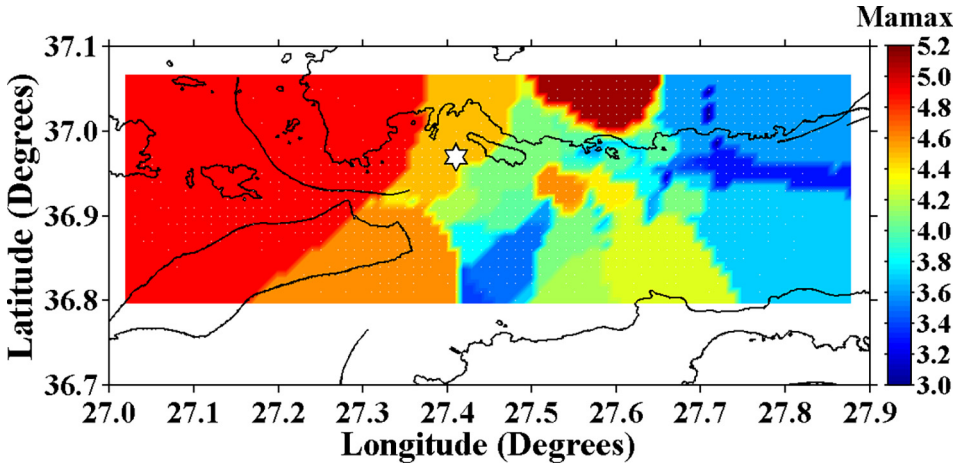

Fig. 11. Spatial distributions of the maximum aftershock magnitudes, Mamax. Mamax maps are plotted by using the same grid and number of aftershocks in each grid node as in the case of *b*-value and *p*-value maps.

the form of rapid evaluations for short term earthquake hazards immediately after the strong/devastating earthquakes, (*viii*) spatial and temporal patterns in aftershock activity may indicate rapid alteration of mainshock-induced stress fields and may define a strong aftershock triggered by the mainshock.

There are not many detailed studies in literature on July 21th, 2017 Bodrum-Kos earthquake and its aftershocks. After the occurrence of this large earthquake, several preliminary reports from different government agencies in Turkey (AFAD, 2017; Kadirioğlu et al., 2017; Alçık et al., 2017; Yalçıner et al., 2017; Heidarzadeh et al., 2017) as well as U.S. Geological Survey (URL-1, 2018) report were prepared. However, one can find some recent information about neotectonic, seismotectonic, geologic and geodynamic evaluations from different studies such as Yolsal-Çevikbilen et al. (2014) and Tur et al. (2015). The July 21th, 2017 Bodrum-Kos earthquake, causing strong wave motions, was resulted in some damages at some small bays in the south of Bodrum peninsula. The mainshock is related to the south striking the Gökova Fault Zone and north-striking Datça fault. Bodrum-Kos earthquake region is also located within the Gökova seismic gap which is determined as seismic gap by Demirtaş and Yılmaz (1996). For this reasons, monitoring the micro seismic activity and analyzing other geophysical parameters such as InSAR (Interferometric Synthetic Aperture Radar) observation and the Coulomb stress analysis may contribute to the evaluation of aftershock hazard after the Bodrum-Kos mainshock. Kadirioğlu et al. (2017) used the InSAR observation technique (data is taken from Sentinel 1A satellite) in order to measure the possible coseismic deformations after the mainshock. In their interferogram (see their Fig. 20), they observed some collapses with approximately 20 cm in Karaada which are located in the north of the Gökova Fault Zone. As discussed above, this region is related to the lower *b*-value and higher *p*-value. Thus, these results are consistent with the findings of other researchers mentioned above. Coulomb stress analysis for the Bodrum-Kos aftershock region was made by Kadirioğlu et al. (2017) and in the preliminary report of AFAD (2017). In the report of AFAD (2017), it is stated that Bodrum-Kos earthquake occurred on the normal fault with a dip N82E-53SE which limited the Gökova Gulf from the north, and a rupture in 20 km length and in 16 km width was occurred after the mainshock. According to Coulomb stress analysis (see their Fig. 11) of AFAD (2017), a stress load between 0.8 and 1.0 bar was observed in the western and eastern end of the fault, whereas stress values show decreases in the north-south direction. Kadirioğlu et al. (2017) made a Coulomb stress analysis before and after Bodrum-Kos earthquake. According to the Coulomb stress analysis before the mainshock, a stress load between 0.3 and 0.5 bar was observed especially in the north of Datça peninsula and around Kos Island (see Fig. 21 of AFAD, 2017). However, in the calculation that the earthquakes with magnitude $M \geq 4.0$ before and after the mainshok were used, a stress load between 0.8 and 1.0 bar was observed in the south of Karaada, and a stress load between 0.4 and 1.0 bar in the north of Karaada in Bodrum peninsula (see Fig. 22 of AFAD, 2017). As seen in Fig. 9a in this study, the lowest *b*-values indicating high positive stress changes are observed in the eastern and western ends of the aftershock region, including Karaada, Bodrum, Turgutreis and Akyarlar as stated in Kadirioğlu et al. (2017) and in the preliminary report of AFAD (2017). Also, the largest *b*-values are generally related to the northeast and southwest parts of the mainshock epicenter, which may have low stress. As a result, the eastern and western ends of the aftershock region have a high stress distribution whereas there is a lower stress changes in the northeast and southwest parts of the aftershock sequence. From epicenter distributions map of aftershocks in this study (Fig. 2), we can see clearly that the majority of the aftershocks occurred in the sea region. For this reason, we did not make a suitable and reliable assessment of *b*-value and *p*-value regarding geological aspect. Also, since no surface rupture of the causative faults were not stated in Bodrum-Kos aftershock region, we did not suggest a relationship between slip and *p*-value. Thus, obtained results in this work among *b*-value, stress changes and coseismic deformation are supported by the general results provided by Wiemer and Katsumata (1999), Enescu and Ito (2002), Bayrak and Öztürk (2004), and Öztürk et al. (2008).

7. Conclusions

A statistical space-time-magnitude analysis for the aftershock sequence of July 21th, 2017 $M_W = 6.5$ Bodrum-Kos, Turkey, earthquake was made. For this purpose, the *b*-value from Gutenberg-Richter law, *p*-value from modified Omori law, *Dc*-value from fractal dimension and Mamax of possible maximum magnitudes in the aftershock sequence were estimated. Earthquake data including 10,600 aftershocks in six months after the mainshock was compiled from AFAD and KOERI. Completeness magnitude for aftershock sequence was considered as $Mc = 1.6$ and *b*-value was calculated as 0.90 ± 0.05. This *b*-value is very close to 1.0 and typical for aftershock sequences. Thus, this aftershock sequence is well represented by the Gutenberg-Richter law and this relatively low *b*-value may be connected with the plenty of larger aftershocks with $M_L \geq 4.0$. *p*-value was obtained as 1.04 ± 0.02 with a *c*-value $= 0.224 \pm 0.039$ by fitting the data for events with $Mmin = 2.3$ and $Tstart = 0.01$. Since aftershock activity shows a relatively fast decay rate, it is estimated a relatively great *p*-value. These results show that no background activity is not included in the calculation and there is not an incompleteness at the beginning of the

sequence according to this *c*-value. Hence, the simple modified Omori law can be considered a suitable model for Bodrum-Kos aftershock sequence. From the estimated fractal dimension, $Dc = 1.74 \pm 0.09$, it can be concluded that the Bodrum-Kos aftershocks are not heterogeneously distributed over a two dimensional fault plane. *b*-values show a temporal decrease before the occurrence of larger aftershocks and it can be interpreted that this decreasing trend in *b*-values may be due to an increase in effective stress.

The spatial distributions of *b*-value change between 0.5 and 1.2. The lowest *b*-values were observed in and around mainshock, including Turgutreis, Akyarlar, Bodrum and Karaada, and these regions are related to high stress regions as well as coseismic deformation regions. Spatial variations in *p*-value vary from 0.4 to 1.3. The largest *p*-values were observed in and around the mainshock epicenter including Karaada, and this situation may be associated with the coseismic deformations in these parts of aftershock sequence. Since there is no slip information, we could not interrelate with *p*-value and rupture mechanism of the aftershock region. Spatial distribution of the maximum aftershock magnitudes Mamax changes between 3.0 and 5.2. There are 50 aftershocks larger than and equal to 4.4 in the catalog. Larger Mamax values were observed in and around mainshock epicenter, including Akyarlar and Bodrum, and a correlation was observed between lower *b*-value distributions and larger Mamax. These results show that there is a correlation among aftershock parameters, stress changes and coseismic deformation, and an effective space-time-magnitude analysis of aftershock sequence is important. As a remarkable fact, these types of preliminary investigations of aftershock occurrences may be crucial for the fast evaluations of real time aftershock hazard in a short-time immediately following strong or devastating earthquakes.

Acknowledgements

Large earthquake information is merged from the earthquake catalogs reported by the AFAD and KOERI. Figs. 1 and 2 in this paper are prepared by using GMT (Generic Mapping Tools) software which is written by Wessel and Smith (1998). The authors would also like to thank to Prof. Dr. Stefan Wiemer for providing ZMAP software and the anonymous reviewers for their useful and constructive suggestions in improving this paper.

References

AFAD, 2017. Preliminary Evaluation Report of July 21th, 2017 Muğla-Bodrum Offshore Earthquake (in Turkish). Disaster and Emergency Management Authority, Ankara.
Aki, K., 1965. Maximum likelihood estimate of b in the formula and its confidence limits. Bull. Earthquake Res. Inst. Tokyo Univ. 43, 237–239.
Alçık, H., Korkmaz, A., Çırağ, O., Şafak, E., 2017. Acceleration records and their properties of July 21, 2017 Kos Islands-Gökova Bay earthquake (in Turkish). Bogazici University, Kandilli Observatory and Earthquake Research Institute, İstanbul.
Ansari, S., 2016. Co-seismic stress transfer and magnitude-frequency distribution due to the 2012 Varzaqan-Ahar twin earthquakes (Mw 6.5 and 6.4), NW Iran. J. Asian Earth Sci. 132, 129–137. https://doi.org/10.1016/j. jseaes.2016.10.006.
Ansari, S., 2017. Aftershocks properties of the 2013 Shonbe Mw 6.3 earthquake, central Zagros, Iran. J. Asian Earth Sci. 147, 17–27. https://doi.org/10.1016/j.jseaes.2017.07.042.
Arora, B.R., Bansal, B.K., Prajapati, S.K., Sutar, A.K., Nayak, S., 2017. Seismotectonics and seismogenesis of Mw7.8 Gorkha earthquake and its aftershocks. J. Asian Earth Sci. 133, 2–11. https://doi.org/10.1016/j.jseaes.2016.07.018.
Ávila-Barrientos, L., Zúñiga, F.R., Rodríguez-Perez, Q., Guzmán-Speziale, M., 2015. Variation of b and p values from aftershocks sequences along the Mexican subduction zone and their relation to plate characteristics. J. S. Am. Earth Sci. 63, 162–171. https://doi.org/10.1016/j.jsames.2015.07.009.
Båth, M., 1965. Lateral inhomogeneities of the upper mantle. Tectonophysics 2, 483–514.
Bayrak, Y., Öztürk, S., 2004. Spatial and temporal variations of the aftershock sequences of the 1999 İzmit and Düzce earthquakes. Earth Planets Space 56, 933–944. https://doi.org/10.1186/BF03351791.
Bender, B., 1983. Maximum likelihood estimation of b-values from magnitude grouped data. Bull. Seismol. Soc. Am. 73, 831–851.
Chung-Han, C., Yih-Min, W., 2013. Maximum magnitudes in aftershock sequences in Taiwan. J. Asian Earth Sci. 73, 409–418. https://doi.org/10.1016/j.jseaes.2013.05.006.
Daniel, G., Marsan, D., Bouchon, M., 2006. Perturbation of the Izmit earthquake aftershock decaying activity following the 1999 Mw 7.2 Düzce, Turkey, earthquake. J. Geophys. Res. 111, B05310. https://doi.org/10.1029/2005JB003978.
Davidsen, J., Gu, C., Baiesi, M., 2015. Generalized Omori-Utsu law for aftershock sequences in southern California. Geophys. J. Int. 201, 965–978. https://doi.org/10.1093/gji/ggv061.
Demirtaş, R., Yılmaz, R., 1996. Türkiye'nin Sismotektoniği. Bayındırlık ve İskan Bakanlığı Afet İşleri Genel Müdürlüğü Deprem Araştırma Dairesi, Ankara.
Enescu, B., Ito, K., 2002. Spatial analysis of the frequency-magnitude distribution and decay rate of aftershock activity of the 2000 Western Tottori earthquake. Earth Planets Space 54, 847–859. https://doi.org/10.1186/BF03352077.
Enescu, B., Enescu, D., Ito, K., 2011. Values of b and p: their variations and relation to physical processes for Earthquakes in Japan and Romania. Rom. J. Phys. 56 (3–4), 590–608.
Frohlich, C., Davis, S., 1993. Teleseismic *b*-values: Or, much ado about 1.0. J. Geophys. Res. 98 (B1), 631–644.
Grassberger, P., Procaccia, I., 1983. Measuring the strangeness of strange attractors. Physics D9, 189–208.
Gutenberg, R., Richter, C.F., 1944. Frequency of earthquakes in California. Bull. Seismol. Soc. Am. 34, 185–188.
Habermann, R.E., 1983. Teleseismic detection in the Aleutian Island arc. J. Geophys. Res. 88 (B6), 5056–5064. https://doi.org/10.1029/JB088iB06p05056.
Hainzl, S., Christophersen, A., Rhoades, D., Harte, D., 2016. Statistical estimation of the duration of aftershock sequences. Geophys. J. Int. 205 (2), 1180–1189. https://doi.org/10.1093/gji/ggw075.
Heidarzadeh, M., Necmioglu, O., Ishibe, T., Yalciner, A.C., 2017. Bodrum-Kos (Turkey-Greece) Mw 6.6 earthquake and tsunami of 20 July 2017: a test for the Mediterranean tsunami warning system. Geosci. Lett. 4 (31), 2–11. https://doi.org/10.1186/s40562-017-0097-0.
Helmstetter, A., Shaw, B., 2006. Relation between stress heterogeneity and aftershock rate in the rate-and-state model. J. Geophys. Res. 111, B07304. https://doi.org/10.1029/2005JB004077.
Hirata, T., 1969. Aftershock sequence of the earthquake off Shikotan Island on January 29, 1968. Geophys. Bull. Hokkaido Univ. 21, 33–43.
Hirata, T., 1989. Fractal dimension of fault systems in Japan: fractal structure in rock fracture geometry at various scales. Pure Appl. Geophys. 131 (1–2), 157–170.
Hu, C., Cai, Y., Liu, M., Wang, Z., 2013. Aftershocks due to property variations in the fault zone: a mechanical model. Tectonophysics 588, 179–188. https://doi.org/10.1016/j.tecto.2012.12.013.
Kadirioğlu, F.T., Kartal, R.F., Demirtaş, R., 2017. 21 Temmuz 2017 Gökova Körfezi Depremi (Bodrum Açıkları), Mw = 6.5, Aktif Tektonik Araştırma Grubu 21. Çalıştayı, 26–28 Ekim 2017, AKÜ.
Kagan, Y.Y., Knopoff, L., 1980. Spatial distribution of earthquakes: the two-point correlation function. Geophys. J. Roy. Astron. Soc. 62, 303–320.
Kisslinger, C., Jones, L.M., 1991. Properties of aftershock sequences in Southern California. J. Geophys. Res. 96 (B7), 11947–11958.
Mandelbrot, B.B., 1982. The fractal geometry of nature. Freeman Press, San Francisco.
Marcellini, A., 1997. Physical model of aftershock temporal behavior. Tectonophysics 277, 137–146.
Mignan, A., Woessner, J., 2012. Estimating the magnitude of completeness for earthquake catalogs. Commun. Online Resour. Stat. Seismicity Anal. https://doi.org/10.5078/corssa-00180805. Available at http://www.corssa.org.
Mignan, A., 2015. Modeling aftershocks as a stretched exponential relaxation. Geophys. Res. Lett. 42, 9726–9732.
Nanjo, K., Nagahama, H., Satomura, M., 1998. Rates of aftershock decay and the fractal structure of active fault systems. Tectonophysics 287, 173–186.
Narteau, C., Byrdina, S., Shebalin, P., Schorlemmer, D., 2009. Common dependence on stress for the two fundamental laws of statistical seismology. Nature 462, 642–645. https://doi.org/10.1038/nature08553.
Nemati, M., 2014. An appraisal of aftershocks behavior for large earthquakes in Persia. J. Asian Earth Sci. 79, 432–440. https://doi.org/10.1016/j.jseaes.2013.10.015.
Nuannin, P., Kulhánek, O., Persson, L., 2012. Spatial and temporal characteristics of aftershocks of the December 26, 2004 and March 28, 2005 earthquakes off NW Sumatra. J. Asian Earth Sci. 46, 150–160. http://dx.doi:10.1016/j.jseaes.2011.12.004.
Ogata, Y., 1983. Estimation of parameters in the modified Omori formula for aftershock frequencies by the maximum likelihood procedure. J. Phys. Earth. 31, 115–124.
Ogata, Y., 2001. Increased probability of large earthquakes near aftershock regions with relative quiescence. J. Geophys. Res. 106, 8729–8744.
Olsson, R., 1999. An estimation of the maximum *b*-value in the Gutenberg-Richter relation. Geodynamics 27, 547–552.
Omori, F., 1894. On after-shocks of earthquakes. J. Coll. Sci. Imp. Univ. Tokyo 7, 111–200.
Öncel, A.O., Main, I., Alptekin, A., Cowie, P., 1996. Spatial variations of the fractal properties of seismicity in the Anatolian fault zones. Tectonophysics 257, 189–202.
Öncel, A.O., Wilson, T.H., 2002. Space-time correlations of seismotectonic parameters and examples from Japan and Turkey preceding the İzmit earthquake. Bull. Seismol. Soc. Am. 92, 339–350. https://doi.org/10.1785/0120000844.
Öztürk, S., Çınar, H., Bayrak, Y., Karslı, H., Daniel, G., 2008. Properties of the aftershock sequences of the 2003 Bingöl, M_D = 6.4, (Turkey) earthquake. Pure Appl. Geophys. 165, 349–371. https://doi.org/10.1007/s00024-008-0300-5.
Öztürk, S., 2009. An application of the earthquake hazard and aftershock probability evaluation methods to Turkey earthquakes. PhD Thesis. Karadeniz Technical University, Trabzon, Turkey (in Turkish with English abstract).
Pailoplee, S., Choowong, M., 2014. Earthquake frequency-magnitude distribution and fractal dimension in mainland Southeast Asia. Earth, Planets Space 66, 8. https://doi.org/10.1186/1880-5981-66-8.
Peng, Z., Vidale, J.E., Ishii, M., Helmstetter, A., 2007. Seismicity rate immediately before

and after mainshock rupture from high-frequency waveforms in Japan. J. Geophys. Res. 112, B03306. https://doi.org/10.1029/2006JB004386.
Polat, O., Eyidogan, H., Haessler, H., Cisternas, A., Philip, H., 2002. Analysis and interpretation of the aftershock sequence of the August 17, 1999, Izmit (Turkey) earthquake. J. Seismolog. 6, 287–306.
Polat, O., Gok, E., Yılmaz, D., 2008. Earthquake hazard of the Aegean Extension region (West Turkey). Turk. J. Earth Sci. 17, 593–614.
Ranalli, G., 1969. A statistical study of aftershock sequences. Ann. Geophys. 22, 359–397.
Scholz, C.H., 2015. On the stress dependence of the earthquake b value. Geophys. Res. Lett. 42. https://doi.org/10.1002/2014GL062863.
Schorlemmer, D., Wiemer, S., Wyss, M., 2005. Variations in earthquake-size distribution across different stress regimes. Nature 437. https://doi.org/10.1038/nature04094.
Tajima, F., Kanamori, H., 1985. Global survey of aftershock area expansion patterns. Phys. Earth. Planet. Inter. 40, 77–134.
Toksöz, M.N., Shakal, A.F., Michael, A.J., 1979. Space-time migration of earthquakes along the North Anatolian Fault Zone and seismic gaps. Pure Appl. Geophys. 117, 1258–1270.
Tosi, P., 1998. Seismogenic structure behavior revealed by spatial clustering of seismicity in the Umbria-Marche Region (central Italy). Ann. Geophys. 41, 215–224.
Tsapanos, T.M., Papazachos, C., Moutafi, Z., Gabrielides, J., Spyrou, T., 1994. Properties of the globally distributed aftershock sequences: emphasis in the Circum-Pasific Belt. Bull. Seism. Soc. Am. XXX/5, 121–158.
Tur, H., Yaltırak, C., Elitez, I., Sarıkavak, K.T., 2015. Pliocene-Quaternary tectonic evolution of the Gulf of Gökova, southwest Turkey. Tectonophysics 638, 158–176. https://doi.org/10.1016/j.tecto.2014.11.008.
Turcotte, D.L., 1992. Fractals and Chaos in Geology and Geophysics. Cambridge Univ. Press, New York, pp. 221.
Utsu, T., Seki, A., 1954. Relation between the area of aftershock region and the energy of mainshock. J. Seismol. Soc. Jpn. II 7, 233–240.
Utsu, T., 1969. Aftershocks and earthquake statistic (I): some parameters which characterize an aftershock sequence and their interrelation. J. Faculty Sci. Hokkaido Univ. Ser. VII 2, 129–195.
Utsu, T., 1971. Aftershocks and earthquake statistic (III): analyses of the distribution of earthquakes in magnitude, time and space with special consideration to clustering characteristics of earthquake occurrence (1). J. Faculty Sci., Hokkaido Univ. Ser. VII (Geophys.) 3, 379–441.
Utsu, T., Ogata, Y., Matsu'ura, R.S., 1995. The centenary of the Omori formula for decay law of aftershock activity. J. Phys. Earth 43, 1–33.
Wei-Jin, X., Jian, W., 2017. Effect of temporal-spatial clustering of aftershocks on the analysis of probabilistic seismic hazard. Chinese J. Geophys.-Chinese Ed. 60 (8), 3110–3118.
Wessel, P., Smith, W.H.F., 1998. New, improved version of generic mapping tools released. EOS Trans. AGU 79 (47), 579. https://doi.org/10.1029/98EO00426.
Wiemer, S., 2001. A software package to analyze seismicity: ZMAP. Seismol. Res. Lett. 72, 373–382.
Wiemer, S., Wyss, M., 1997. Mapping the frequency-magnitude distribution in asperities: an improved technique to calculate recurrence times. J. Geophys. Res. 102, 15115–15128.
Wiemer, S., Katsumata, K., 1999. Spatial variability of seismicity parameters in aftershock zones. J. Geophys. Res. 104 (B6), 13135–13151.
Wiemer, S., Wyss, M., 2000. Minimum magnitude of completeness in earthquake catalogs: examples from Alaska, the Western United States, and Japan. Bull. Seismol. Soc. Am. 90 (3), 859–869. https://doi.org/10.1785/0119990114.
Yadav, R.B.S., Papadimitriou, E., Karakostas, V.G., Shanker, D., Rastogi, B.K., Chopra, S., Singh, A.P., Kumar, K., 2011. The 2007 Talala, Saurashtra, western India earthquake sequence: tectonic implications and seismicity triggering. J. Asian Earth Sci. 40, 303–314. https://doi.org/10.1016/j.jseaes.2010.07.001.
Yadav, R.B.S., Gahalaut, V.K., Chopra, S., Shan, B., 2012. Tectonic implications and seismicity triggering during the 2008 Baluchistan, Pakistan earthquake sequence. J. Asian Earth Sci. 45, 167–178. https://doi.org/10.1016/j.jseaes.2011.10.003.
Yalçıner, A.C., Annunziato, A., Papadopoulos, G., Dogan, G.G., Guler, H.G., Cakir, T.E., Sozdinler, C.O., Ulutas, E., Arikawa, T., Suzen, L., Kanoglu, U., Guler, I., Probst, P., Synolakis, C., 2017. The 20th July 2017 (22:31 UTC) Bodrum/Kos earthquake and tsunami; post tsunami field survey report. < http://users.metu.edu.tr/yalciner/july-21-2017-tsunami-report/Report-Field-Survey-of-July-20-2017-Bodrum-Kos-Tsunami.pdf > (accessed on 4 Dec 2017).
Yolsal-Çevikbilen, S., Taymaz, T., Helvacı, C., 2014. Earthquake mechanisms in the Gulfs of Gökova, Sığacık, Kuşadası, and the Simav Region (western Turkey): neotectonics, seismotectonics and geodynamic implications. Tectonophysics 635, 100–124. https://doi.org/10.1016/j.tecto.2014.05.001.
Zhang, S., Wang, G., Sa, W., 2013. Damage evaluation of concrete gravity dams under mainshock–aftershock seismic sequences. Soil Dyn. Earthquake Eng. 50, 16–27. https://doi.org/10.1016/j.soildyn.2013.02.021.
URL-1, 2018. < https://earthquake.usgs.gov/earthquakes/eventpage/us20009ynd#executive > .